Phonon wave propagation in ballistic-diffusive regime

Dao-Sheng Tang (唐道胜), Yu-Chao Hua (华钰超), Ben-Dian Nie (聂本典), and Bing-Yang Cao (曹炳阳)[a)]
Key Laboratory for Thermal Science and Power Engineering of Ministry of Education, Department of Engineering Mechanics, Tsinghua University, Beijing 100084, People's Republic of China

(Received 15 January 2016; accepted 9 March 2016; published online 22 March 2016)

Wide applications of ultra-short pulse laser technique in micromachining and thermophysical properties' measurements make the study on ultrafast transient thermal transport necessarily essential. When the characteristic time is comparable to the phonon relaxation time, phonons propagate in ballistic-diffusive regime and thermal wave occurs. Here, ultrafast transient phonon transport is systematically investigated based on the Monte Carlo (MC) simulations, the Cattaneo-Vernotte (C-V) model, and the phonon Boltzmann transport equation (BTE). It is found that remarkable differences exist between the C-V model and the MC simulations when describing the evolution of the thermal wave excited by the ultra-short heat pulse. The C-V model predicts a non-dispersive dissipative thermal wave, while the MC simulation with Lambert emission predicts a dispersive dissipative thermal wave. Besides, different phonon emissions can significantly influence the evolution of the thermal wave in the MC simulations. A modified C-V model with a time- and position-dependent effective thermal conductivity is derived based on the phonon BTE to characterize the evolution of the transport regime from ballistic to diffusive. The integrations on moments of the distribution function cause the loss of the information of the phonon distribution in wave vector space, making the macroscopic quantities incomplete when describing the ballistic transport processes and corresponding boundary conditions. Possible boundary conditions for the phonon BTE in practice are also discussed on different heating methods. © *2016 AIP Publishing LLC*.
[http://dx.doi.org/10.1063/1.4944646]

I. INTRODUCTION

The ultra-short pulse laser technique has become the effective tool in micromachining[1–4] and thermophysical property measurements.[1,2,5–8] Generally, Fourier's law of heat conduction, with feature of diffusion, is the constitutive equation used for describing the macroscale thermal transport and indicates that heat propagates in diffusive regime. However, for ultrafast heat conduction, Fourier's law predicts an infinite transport speed of the thermal disturbance, deviating from the experimental results which show that heat propagates as thermal waves.[9,10] For transient heat conduction in nanofilms where the characteristic length and time are comparable to the phonon mean free path and the phonon relaxation time, respectively, phonons propagate also as thermal waves in the ballistic-diffusive regime.[11]

Studies on thermal waves are mainly focused on theoretical modeling and simulations due to the difficulty in experimental research. In the past decades, several phenomenological models have been proposed. A hyperbolic heat conduction equation which predicts the wave propagation of the heat pulse was obtained by combining the energy conservation equation and the C-V model proposed by Cattaneo and Vermotte.[12,13] Joseph and Preziosi extended the C-V model with a Jefferys type relaxation integral kernel.[9] Tzou proposed a dual-phase-lagging model considering the mutual delay between heat flux and temperature gradient.[10] Recently, Majumdar[14] and Chen[15] derived the phonon radiation transport equation and the ballistic-diffusive heat conduction equation, respectively, as the substitutes of the phonon Boltzmann transport equation (BTE) in describing the nanoscale transient heat conduction. Guo *et al*. studied the thermal wave based on the thermomass model.[16–18] Ordonez-Miranda *et al*. presented a constitutive equation of the heat flux and temperature with the exact solutions of the phonon BTE.[19] Besides, simulation approaches, including molecular dynamics (MD) simulation, Monte Carlo (MC) simulation, and lattice Boltzmann method (LBM), are also used for thermal wave research. Tsai and MacDonald performed the MD simulations on the transient propagation of the heat pulse in body-centered-cubic crystal at high temperature and found that the energy propagates in the form of wave attached to the diffusive backgrounds.[20] Kim *et al*. investigated the propagation of the heat pulse in multiwall carbon nanotube using the MD simulation.[21] Yao and Cao first studied the propagation of the heat pulse in graphene by MD simulations and indicated that the heat pulse propagates in ballistic-diffusive regime.[22] Xu and Wang developed a LBM scheme with which he studied the ultrafast process of the pico- and femto-second pulse laser heating process in single-crystal silicon and pointed out that the parabolic equation and the hyperbolic equation are neither applicable to the ballistic condition due to the failure of the continuum and local equilibrium approximation.[23] While it is difficult to solve the BTE at transient condition directly, Hua *et al*. solved the BTE by MC technique to study the transient

[a)]Author to whom correspondence should be addressed. Electronic mail: caoby@tsinghua.edu.cn. Tel./Fax: +86-10-6279-4531.

condition in nanofilm and concluded that the thermal disturbance propagates with finite speed and the thermal wave is related to the ballistic transport.[24]

Theoretically, the thermal wave is often involved in second sound[25–31] dominated by phonon normal scatterings (N scatterings) and ballistic thermal wave[24,32–34] dominated by phonon ballistic transport, which is not distinguished in theoretical modeling works.[9,10,12,13,16–18] For the generation of second sound, it is required that $\tau_N \ll t \ll \tau_R$ to make sure of enough N scatterings and avoid the momentum loss caused by resistive scatterings (R scatterings), where t is the characteristic time of thermal transport, τ_N is the relaxation time of the N scattering, and τ_R is the R scattering. Different from the time window for second sound, $t \ll \tau_R \ll \tau_N$ is required for ballistic thermal wave to avoid scatterings and make sure that phonons transport in the ballistic regime. In fact, time conditions of second sound are barely satisfied for nonmetal materials, such as silicon and germanium. In ultrafast thermal transport in nanofilms where the characteristic length and time in the order of nanometers and picoseconds, respectively, the ballistic thermal wave occurs.[11] While theoretical models for ballistic thermal wave are mostly based on the phonon BTE or have relations with the phonon BTE, systematic comparative studies on models and the phonon BTE in describing the phonon wave propagations in ballistic-diffusive regime are crucial for understanding the ballistic thermal wave.

Boundary conditions play an important role in phonon ballistic-diffusive transport. Although there have been some modifications on macroscopic boundary conditions,[35] there is few discussion on boundary conditions of the phonon distribution function for the phonon BTE. The equilibrium distribution functions at corresponding temperature are usually chosen to be the microscopic boundary conditions.[14,15,19] However, Wilson and Cahill indicated that the radiative boundary condition is not an accurate description for interface thermal resistance at ballistic transport.[36] An anisotropic distribution function $f = f(T_1) - \tau_R v_x \partial f/\partial x(T_1$ is the temperature of the phonon source) was set up as the boundary condition in dealing with the nanoscale interface transport.[11] Boundary conditions of the distribution function at ultrafast transient transport and their influences on ballistic transport have not been investigated systematically yet.

In the present work, we studied the propagation of the ultra-short heat pulse using the MC simulation and the C-V model together with theoretical analyses based on the phonon BTE with relaxation time approximation (RTA). A modified C-V model with a time- and position-dependent effective thermal conductivity (ETC) is derived based on the phonon BTE to characterize the evolution of the transport regime from ballistic to diffusive. The failure of the macroscopic quantities when describing the ballistic transport and its boundary conditions is pointed out and proven based on their definitions and results of the MC simulations. Possible boundary conditions of distribution function for the phonon BTE in practice and corresponding emissions in MC simulations are discussed.

II. SIMULATION AND NUMERICAL METHODS

A. Monte Carlo simulation

A Monte Carlo technique,[37,38] which directly solves the phonon BTE by simulating the corresponding physical processes, is employed to investigate the phonon ballistic-diffusive transport. As presented in Fig. 1, one-dimensional transient heat conduction in single-crystal silicon nanofilms is simulated. The heat pulse propagates along the normal direction of the boundary (x-direction). There are no confinements in y- and z-directions. Thus, the initial temperature, T_0, is 300 K, and a heat pulse with period $\Delta t = 2$ ps is input to the left side of the film at $t = 0$. Phonons scatter at the boundary and are reflected back to the film diffusively. The phonon-phonon scattering is treated in RTA. Phonons emit in two different ways: the directional emission (DE) (all phonons are emitted with the same direction expressed by the angle θ between the emission direction and the boundary normal direction) and the Lambert emission (LE) (phonons are emitted with angular distribution based on the Lambert cosine law). The temperature is calculated based on its relation with the number of phonons scattered in the corresponding cell (the thin film is divided into 1000 cells uniformly), and more details of the simulation can be referred to Refs. 24, 37, and 38. The heat flux density at the boundary is set based on its definition: energy (phonons) transmitting the specific interface per time and per area. The definition of the heat flux in MC simulation with LE and DE is

$$E_{LE} = \sum_{p=1}^{3} \int_{\Omega} \int_{\omega} \hbar \omega f v_{LE} \cos(\theta) \mathrm{DOS} d\omega d\Omega, \tag{1}$$

$$E_{DE} = \sum_{p=1}^{3} \int_{\Omega} \int_{\omega} \hbar \omega f v_{DE} \mathrm{DOS} d\omega d\Omega, \tag{2}$$

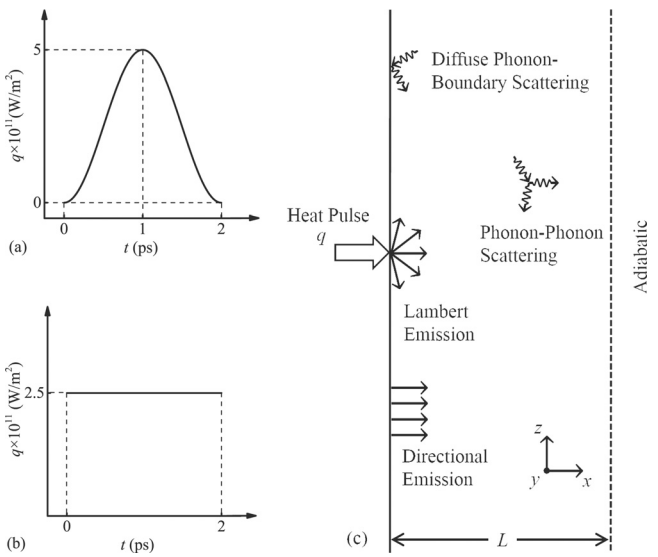

FIG. 1. Schemes of the heat pulse and the system of Monte Carlo simulation for single-crystal silicon nanofilm: (a) sinusoidal heat pulse, (b) rectangle heat pulse, and (c) simulation system including the regimes of phonon emission and scattering.

respectively, where $\cos(\theta)$ corresponds to the Lambert emission. v_{LE} and v_{DE} are the velocities of phonons when transmitting the interface. The condition $E_{LE} = E_{DE}$ is guaranteed in our simulations by emitting same phonon bundles (phonons with specific energy) at same time interval. After the phonon emission, phonons propagate as phonon group velocity.

Debye approximation is adopted for phonon frequency spectrum and dispersion relation.[38] Phonon polarization and anisotropy of the crystal structure are not considered. The phonon group velocity, v_q, which is set to be the phonon velocity in simulation, and the phonon MFP, l, is set to be 5000 m/s and 56.2 nm, respectively.[11] The phonon relaxation time is then calculated to be 11.2 ps. The specific heat capacity, c_v, and the density, ρ, of the bulk material at initial temperature are used in simulations for the nanofilm. The film thickness, L, is set to be 120 nm and 1000 nm, respectively, in simulations according to the changes of the characteristic time in research. The role of the opposite boundary is not considered in this research.

In the present work, we investigate the heat flux pulse condition which has been widely adopted in experimental and numerical studies.[5–8,16–18,39] As shown in Figs. 1(a) and 1(b), the pulse function are selected to be sinusoidal and rectangle functions, respectively

$$q_1 = \begin{cases} q_{max} \times \frac{1}{2}\left(1-\cos(\omega_{p0} t)\right), & t < t_0 \\ 0, & t \geq t_0, \end{cases} \tag{3}$$

$$q_2 = \begin{cases} q_{max} \times \frac{1}{2}, & t < t_0 \\ 0, & t \geq t_0, \end{cases} \tag{4}$$

where $q_{\max} = 5 \times 10^{11}\ \mathrm{W/m^2}$, $t_0 = 2$ ps, and $\omega_{p0} = 3.14\ \mathrm{rad\ ps^{-1}}$ with initial conditions

$$\begin{aligned} &T = T_0,\ t = 0, \quad 0 \leq x \leq L, \\ &q = 0,\ t = 0, \quad 0 \leq x \leq L. \end{aligned} \tag{5}$$

B. Numerical method for the C-V model

The C-V model

$$q + \tau_{CV} \frac{\partial q}{\partial t} = -\lambda \frac{\partial T}{\partial x}, \tag{6}$$

where λ is the thermal conductivity and τ_{CV} is the relaxation time, is often used as the alternative constitutive heat conduction equation to Fourier's law at ultrafast condition. In this text, a numerical computation method is adopted to solve the one-dimensional C-V equation under the same initial and boundary conditions with those in MC simulations. A dimensionless method is adopted to simplify the numerical calculation process. The dimensionless position x^*, time t^*, temperature T^*, heat flux q^*, and characteristic time Z_τ are, respectively, defined as

$$\begin{aligned} &x^* = x/d, \quad t^* = t/(d^2/\alpha), \quad T^* = T/T_0, \\ &q^* = q/(\lambda T_0/d), \quad Z_\tau = \tau_{CV}/(d^2/\alpha), \end{aligned} \tag{7}$$

where d is the thickness of the thin film, and α is the thermal diffusivity. The one-dimensional C-V equation and the one-dimensional energy conservation equation without heat sources can be transformed to be the dimensionless form as follows:

$$Z_\tau \frac{\partial q^*}{\partial t^*} + \frac{\partial T^*}{\partial x^*} = -q^*, \tag{8}$$

$$\frac{\partial T^*}{\partial t^*} + \frac{\partial q^*}{\partial x^*} = 0. \tag{9}$$

To get a more accurate result on temperature profiles, the high-order purely numerical explicit total-variation-diminishing (TVD) scheme with Roe's superbee limiter function[39,40] is used in this work. Eqs. (8) and (9) can be rewritten as the dimensionless vector form

$$\frac{\partial \mathbf{U}}{\partial t^*} + \frac{\partial \mathbf{F}}{\partial x^*} = \mathbf{S}, \tag{10}$$

with the vectors defined as

$$\mathbf{U} = \begin{bmatrix} Z_\tau q^* \\ T^* \end{bmatrix}, \quad \mathbf{F} = \begin{bmatrix} T^* \\ q^* \end{bmatrix}, \quad \mathbf{S} = \begin{bmatrix} -q^* \\ 0 \end{bmatrix}. \tag{11}$$

With the method of diagonalization based on eigenvalue,[40] a new variable vector is defined as

$$\mathbf{W} = \begin{bmatrix} \frac{1}{2}\left(T^* + \sqrt{Z_\tau} q^*\right) \\ \frac{1}{2}\left(T^* - \sqrt{Z_\tau} q^*\right) \end{bmatrix}, \tag{12}$$

and Eqs. (8) and (9) can be rewritten as

$$\frac{\partial W}{\partial t^*} + \boldsymbol{\lambda} \frac{\partial W}{\partial x^*} = \mathbf{R}, \tag{13}$$

where

$$\boldsymbol{\lambda} = diag\left(\frac{1}{\sqrt{Z_\tau}}, -\frac{1}{\sqrt{Z_\tau}}\right), \tag{14}$$

$$\mathbf{R} = \left[-\frac{q^*}{2\sqrt{Z_\tau}}, \frac{q^*}{2\sqrt{Z_\tau}}\right]^T. \tag{15}$$

Thus, coupled equations of heat flux q and temperature T can be transformed into equations, respectively, for W_j $(j = 1,2)$, which can be readily solved by the TVD scheme with the Roe's superbee limiter function.[40]

Verification is made by comparing our dimensionless results with those in Ref. 39, illustrated in Fig. 2, in solving the one-dimensional heat conduction problem under the same initial and boundary conditions. The model in Ref. 39 is based on the thin film which is finite in x-direction and infinite in y- and z-directions, with the boundary and initial conditions

$$q^* = \begin{cases} 1 - \cos(2\pi t^*/0.05), & x^* = 0, \quad t^* < 0.05 \\ 0, & x^* = 0, \quad t^* \geq 0.05, \end{cases} \tag{16}$$

$$\begin{aligned} &T^* = 1, \quad t^* = 0, \quad 0 \leq x^* \leq 1, \\ &q^* = 0, \quad t^* = 0, \quad 0 \leq x^* \leq 1. \end{aligned} \tag{17}$$

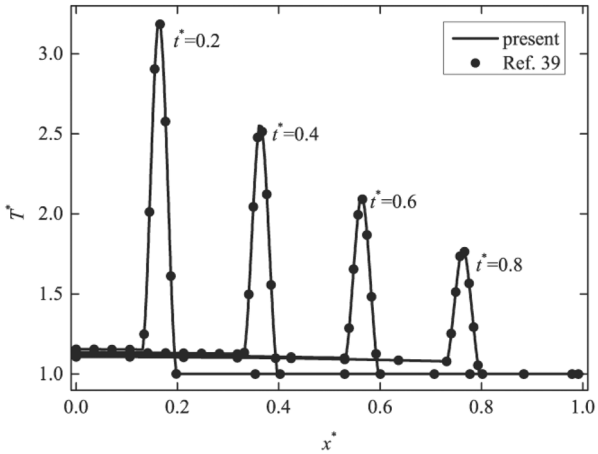

FIG. 2. Comparison between the spatial dimensionless temperature distribution calculated by numerical method in this work and that in Ref. 39.

Good agreement of the results in the present work with those in Ref. 39 proves the validity of this method.

III. RESULTS AND DISCUSSION

A. Temperature distribution

The temperature profiles calculated by the MC simulations with LE and DE ($\theta = 0°$) are shown in Figs. 3 and 4, respectively. The results of the C-V model are also plotted in comparison with those of the MC results. The C-V model predicts a non-dispersive dissipative thermal wave with dispersion relation

$$\omega_t = \frac{\sqrt{3}}{3} v_q k_t, \tag{18}$$

where ω_t and k_t are the frequency and the wave vector of the thermal wave, respectively, and the velocity of the wave front and the wave peak are both equal to $\sqrt{3}v_q/3$. The dispersion relation can be derived from the wave equation of temperature of the C-V model

$$\frac{\partial^2 T}{\partial t^2} + \frac{1}{\tau_R}\frac{\partial T}{\partial t} = \frac{\lambda}{\tau_R \rho c_V}\frac{\partial^2 T}{\partial x^2}, \tag{19}$$

where

$$\lambda = \frac{1}{3} v_q{}^2 \tau_R \rho c_V. \tag{20}$$

Eq. (19) predicts a monochromatic dissipative wave with wave velocity $\sqrt{3}v_q/3$ and dispersion relation $\omega_t = \frac{\sqrt{3}}{3} v_q k_t$ obtained by making spatial and temporal Fourier transform on Eq. (20). Much differently, the MC simulation with LE predicts a dispersive dissipative thermal wave with dispersion relation

$$\omega_t = v_q \cos(\theta) k_t, \quad 0° < \theta < 90°, \tag{21}$$

and the velocity of the wave front equates to v_q. For the MC simulations, considering the phonon BTE without scattering term, we have

$$\frac{\partial f}{\partial t} + v_q \cos(\theta)\frac{\partial f}{\partial x} = 0. \tag{22}$$

The dispersion relations of the temperature profiles and the distribution profiles are the same because the temperature has a linear relation with the distribution function. By taking spatial and temporal Fourier transform, the dispersion relation of Eq. (22) is obtained as shown in Eq. (21) in which θ distributes according to the Lambert cosine law. Obviously, resulting from the superposition of phonon waves with different directions, ω_t is not the single value function of k_t, which is different from the simple dispersion relations. For the MC simulations with DE, $\theta = \theta_0$, the dispersion relation becomes

$$\omega_t = v_q \cos(\theta_0) k_t. \tag{23}$$

Waveform of the heat pulse is not kept during the propagation process and barely influences the shapes of the temperature profiles in MC simulations with LE, as shown in Figs. 3(a) and 3(b). Besides, the simulated thermal wave peak value attenuating rapidly in the first 10 ps is much lower than that in the C-V model, because in the MC simulations with LE the energy propagates as a dispersive wave and can be distributed more uniformly in heated region along the x

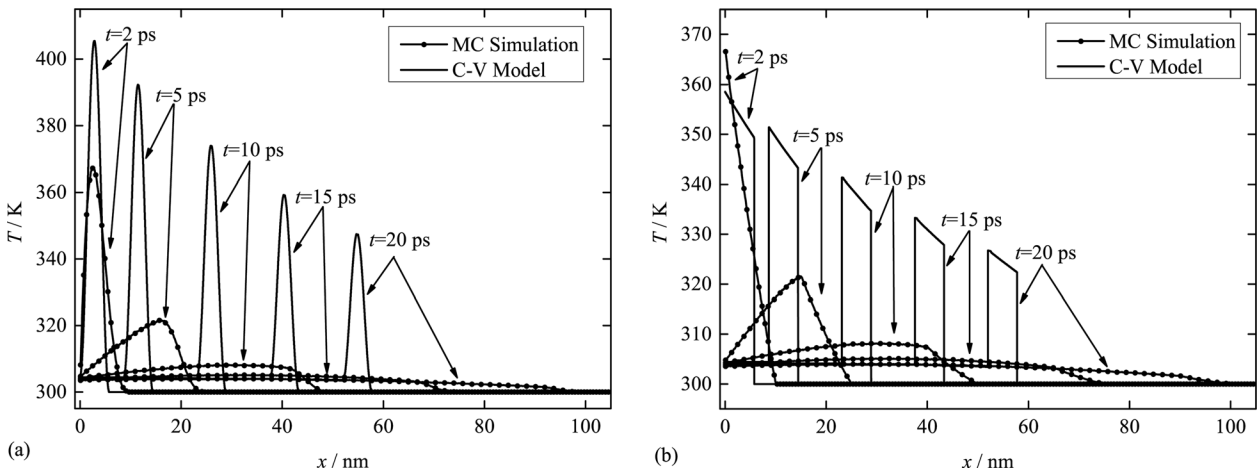

FIG. 3. Temperature distribution profiles calculated by MC simulations with LE and the C-V model under the stimulation of (a) sinusoidal heat pulse and (b) rectangle heat pulse.

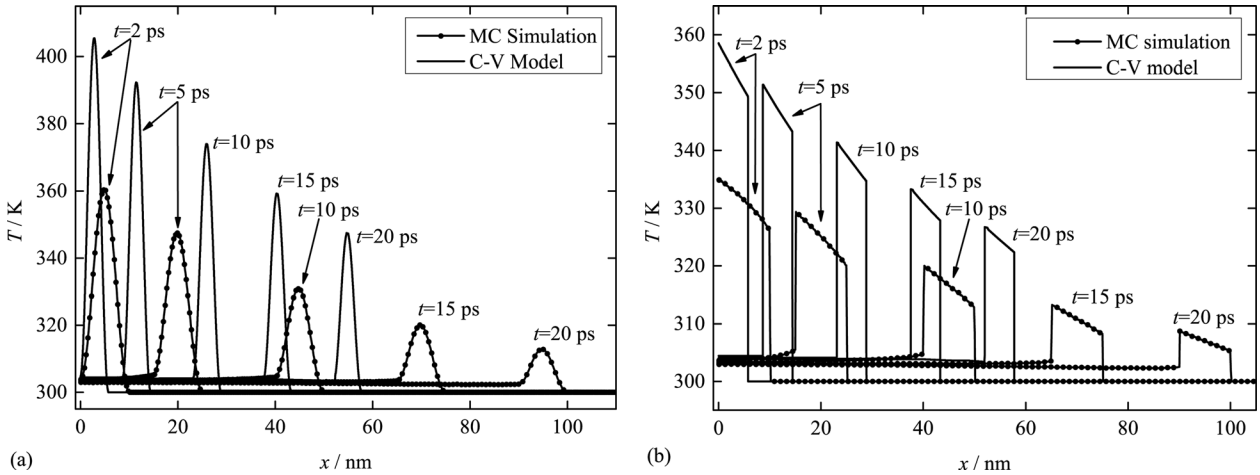

FIG. 4. Temperature distribution profiles calculated by MC simulations with DE and the C-V model under the stimulation of (a) sinusoidal heat pulse and (b) rectangle heat pulse.

direction. In contrast, for the C-V model, the energy is obviously concentrated near the wave peak, leading to higher max-temperature in practical applications. In the MC simulations, the temperature profiles become much different as the phonon emission is changed to be DE ($\theta = 0°$), as illustrated in Figs. 4(a) and 4(b). The heat pulse propagates as a monochromatic dissipative thermal wave with dispersion relation

$$\omega_t = v_q \cos(\theta) k_t, \quad \theta = 0°, \tag{24}$$

and the velocity of the wave front and the wave peak are both equal to v_q. Seen from Figs. 4(a) and 4(b), the propagation of the heat pulse in the predictions of MC simulations with DE is much similar to that in those of the C-V model except the wave velocity.

The temperature-time profiles at specific positions are mostly measured in experiments due to the difficulty in measuring the temperature-position profiles.[5–8] As shown in Figs. 5(a)–5(c), the temperature profiles at specific positions for sinusoidal heat pulse condition are calculated by the MC simulations with two emissions and the C-V model, respectively. The pulse width (PW) t_{PW} is employed as a time parameter in describing the temperature profiles and the heat pulse which is defined as

$$t_{\mathrm{PW}} = t_2 - t_1, \quad t_2 > t_1, \tag{25}$$

with

$$Q(t_1) = Q(t_2) = 0.5 Q_{max}, \tag{26}$$

where Q represents the corresponding physical quantity, i.e., temperature T and heat flux density q for temperature profiles and heat pulse, respectively. The PW of the sinusoidal heat pulse is calculated to be 1 ps. Comparisons between the PWs of temperature profiles and the heat pulse are also shown in Figs. 5(a)–5(c). For the results of the MC simulations with LE, the PW of the temperature profile at $x = 11$ nm ($Kn = 5$, $Kn = l/x$) is larger than that of the heat pulse and increases with the increasing of x. The ballistic transport of the delta function heat pulse from a point source to a point sensor has been studied considering the frequency-dependent phonon properties,[41] and the temperature-time profile at the point sensor which was calculated using the Laudauer formula is similar to that in Fig. 5(a) at $x = 11$ nm where the ballistic transport is significant. The broadening of the PWs both in Ref. 41 and in Fig. 5(a) indicates the dispersion of the thermal wave, i.e., that there are wave components with different wave velocities. In the predictions of MC simulations with DE, the temperature profiles are the same as those from the C-V model both in shapes of profiles and PWs which are equal to that of the heat pulse.

By changing the phonon velocity to $\sqrt{3}v_q/3$, same results of the temperature distribution as those from C-V model are obtained by the MC simulations with DE ($\theta = 0°$), which are shown in Figs. 6(a) and 6(b). The harsh terms needed for getting the consistent results in simulations indicate the limits of the classical thermal wave equation and the macroscopic boundary conditions when describing the ballistic transport. During the period of the heat pulse, phonons of different emission directions are excited at the boundary, and phonons of same emission direction have the same x-components' velocity. As illustrated in Figs. 7(a)–7(c), the pulse of phonons of same emission direction propagates as a monochromatic thermal wave attached to the diffusive background with the wave peak velocity $v_p = v_q \cos(\theta_0)(\theta_0 = \text{const.})$ and the dispersion relation $\omega_t = v_q \cos(\theta_0) k_t$. However, the propagation speed of the thermal disturbance or the wave front v_f are always equal to v_q whatever the angle is in simulations with DE, which is attributed to these phonons who transport in direction of the increasing of x in ballistic regime after the first phonon-phonon scattering near the boundary. As illustrated by the simulation results in Figs. 3 and 7, the temperature profiles calculated by simulations with LE are the cosine-weighted superposition of all possible profiles calculated by simulations with DE (the angle ranges from 0° to 90°). The superposition results in serious dispersions of thermal waves and broadening of PWs in simulations with LE stated above which would be aggravated once the frequency dependence of the phonon group velocity are taken into considerations.[41]

Due to that the temperature profiles of the thermal wave obtained from the C-V model and the MC simulation with DE are similar with the temperature wave[22,42] in cases of

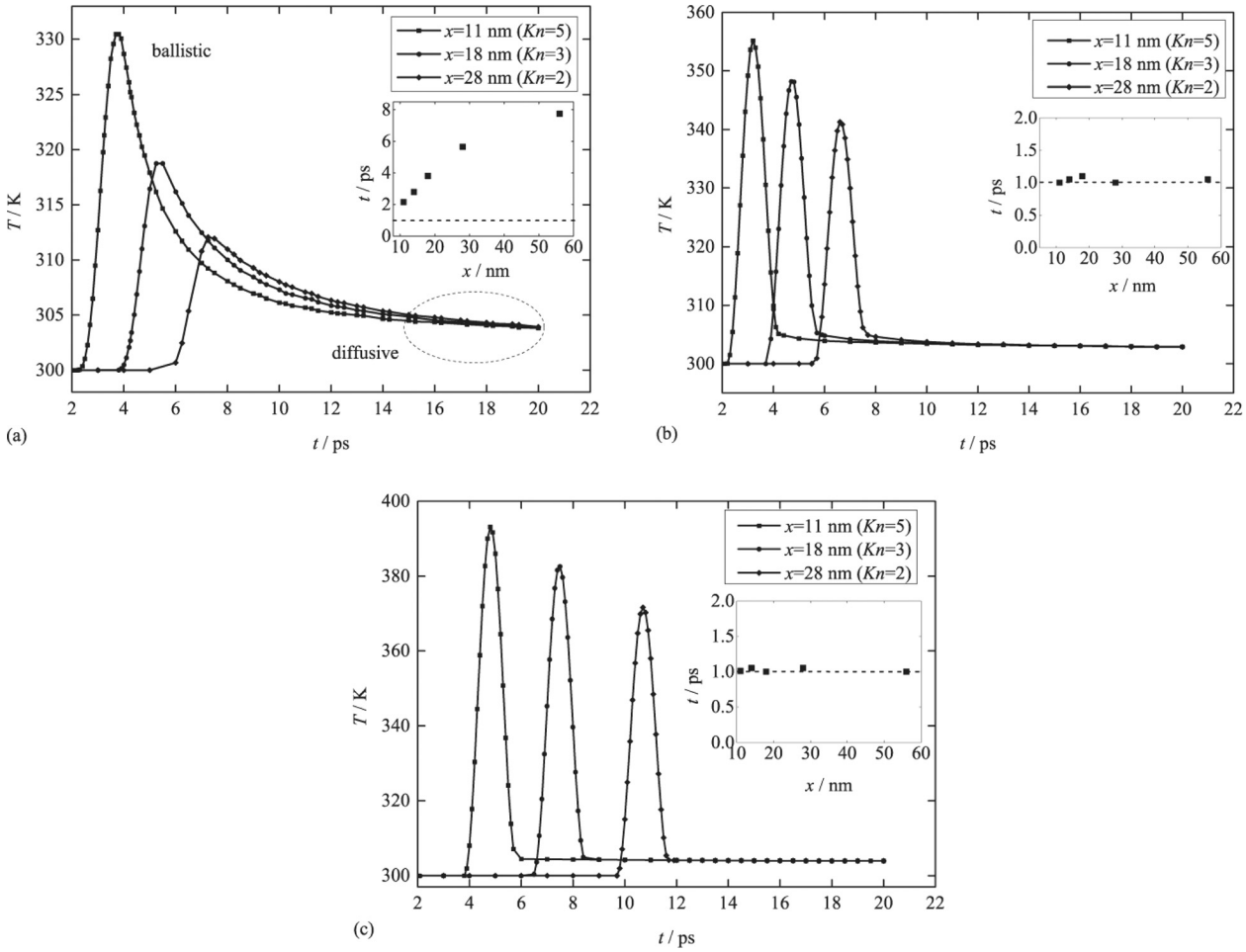

FIG. 5. Temperature profiles at specific positions and PWs calculated by (a) MC simulation with LE, (b) MC simulation with DE, and (c) the C-V model. The rectangle dots represent the PWs of the temperature profiles.

Fourier heat conduction, it should be noted that the thermal wave and the temperature are actually quite different. The thermal wave in ultrafast thermal transport (we call it ballistic thermal wave) is due to the ballistic transport of heat, while the temperature wave resulting from the periodic boundary condition is still under the regime of diffusive transport and just a kind of transient case of the Fourier heat conduction. For the temperature wave, the wave velocity is determined by period of the boundary condition and the thermal diffusivity of the materials. However, the wave velocity is only determined by the properties of the materials (especially the phonon group velocity) for thermal wave.[22,42]

In the case shown in Fig. 8 where the characteristic time (200 ps) and the corresponding characteristic length (1000 nm)

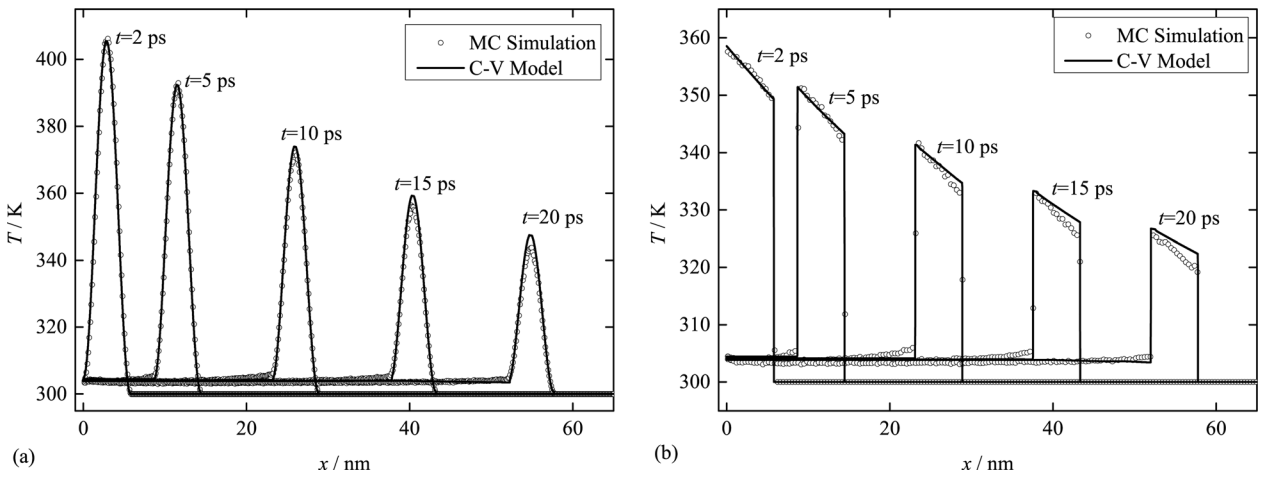

FIG. 6. Matching curves of results of MC simulations under specific simulation condition with those of the C-V model: (a) sinusoidal heat pulse and (b) rectangle heat pulse.

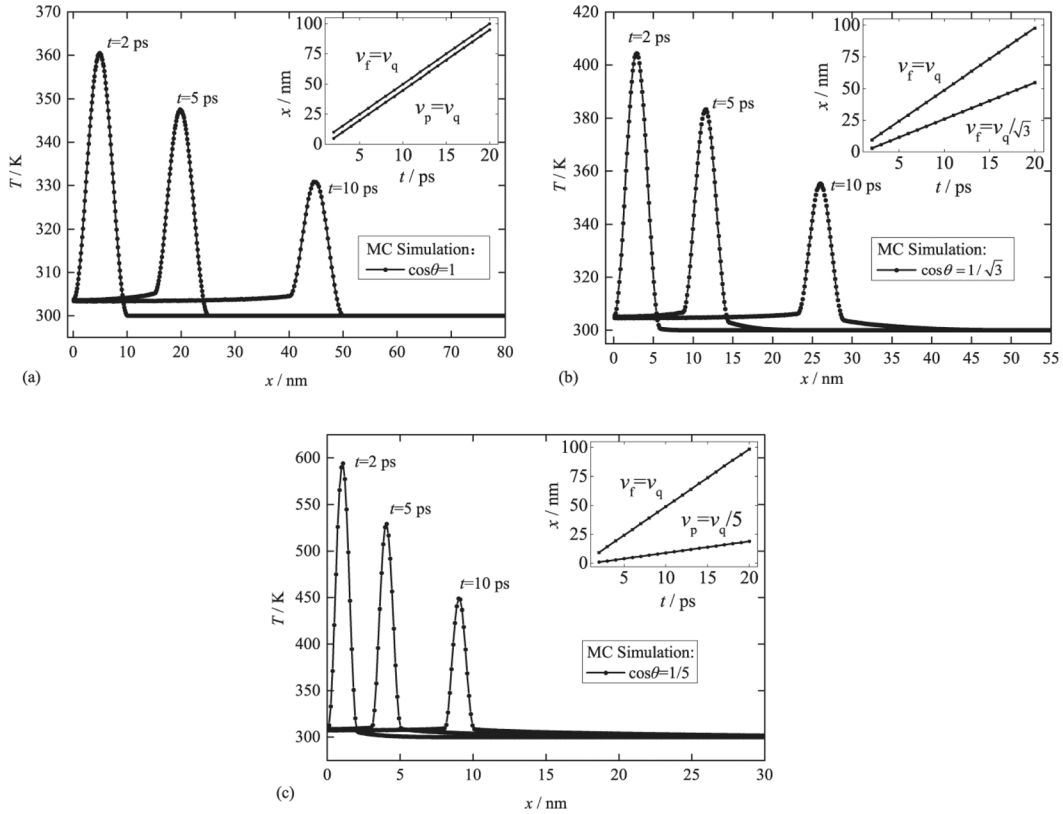

FIG. 7. Temperature distribution profiles calculated by MC simulations with DE: (a)$\cos\theta = 1$, (b)$\cos\theta = 1/\sqrt{3}$, and (c)$\cos\theta = 1/5$, and comparisons between v_f and v_p in the attached figures at the top of the right corner.

are much larger than the phonon relaxation time (11.2 ps) and the phonon MFP (56.2 nm), respectively, phonons transport in the diffusive regime, and the results of the temperature distribution calculated by the MC simulations and the C-V model tend into uniform. The emissions in the simulations do not influence the temperature profiles anymore. The results in Fig. 8 show that the diffusive thermal transport is well described by the classical thermal wave model with macroscopic boundary conditions.

There are actually a few other macroscopic thermal wave models, including the DPL model,[10] the TM model,[16–18] and the GK model.[31] However, as phenomenological models, the DPL model and the TM model do not indicate clear regime of the thermal wave. While the DPL model contains the phonon relaxation time of normal scattering process and the TM model has relations with phonon hydrodynamics which is dominated by phonon normal scattering process,[17] these two models tend to predict the second sound. At specific conditions, these two models can degenerate to the C-V model.[18] The GK model is directly derived from the phonon BTE with R and N processes' terms and predicts the second sound.[31] The two-temperature models, including hyperbolic one/two-step models[43] and parabolic one/two-step models,[44,45] expressed the two processes: electron system is heated by absorbing the photons, and phonon system is heated by electron-phonon coupling. Works on experimental studies on thermal wave or ultrafast heat conduction were carried in last several decades.[25–29,42,46] As stated in the Introduction, the experiments on the second sound in helium,[25–27] NaF,[28] and other liquids and solids[29] are based on phonon BTE with both R and N processes which corresponds to the GK model theoretically. The thermal wave in metal thin films[42,46] have been studied with time-domain thermoreflectance (TDTR) measurements' experiments which are the main ultrafast heat conduction experiments. However, the electron and phonon systems are both included in experiments when semiconductor and dielectric solids are measured and only electron temperature in front surface of thin metal film (the transducer) can be gathered.[5–8] In this work, the MC simulation and the theoretical analysis are based on the phonon BTE with only resistive scattering term, and the ballistic-diffusive thermal transport in single-crystal silicon where the ballistic thermal

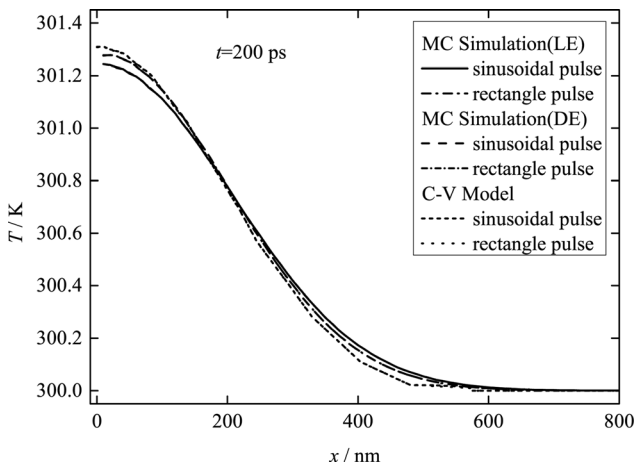

FIG. 8. Temperature distribution profiles at 200 ps calculated by MC simulations and the C-V model.

wave occurs is investigated. And also, we are not aiming to make a complete investigation on an actual ultrafast heat conduction process but on regime of ballistic thermal wave. Thus, the simulation results are not compared with some other macroscopic models due to difference in theoretical bases and experiments due to limitation of available experimental data.

The temperature results obtained above and the comparisons between them involved in the comparisons between the C-V model and the MC simulations with different emissions in predicting the temperature distributions indicate the defects of the C-V model in describing the ballistic transport and some new views on ultrafast thermal transport research. The difference between the MC simulation and the C-V model does not result from the numerical treatments of the boundary condition. Different treatments for the same macroscopic boundary condition reflect different physical details at boundary, which cannot be reflected in the macroscopic boundary condition of the C-V model. While the inapplicability of the C-V model is often attributed to the diffusive approximation,[11] the modification for the C-V model is required for further understanding. What's more, the macroscopic boundary condition is required to be analyzed by its definition. Finally, possible boundary conditions at microscopic level for the phonon BTE should be illustrated.

B. On diffusive approximation of the phonon BTE

Considering the RTA and the R scattering process only, the one-dimensional phonon BTE is[11]

$$\frac{\partial f}{\partial t}+v_x\frac{\partial f}{\partial x}=\frac{f_0-f}{\tau_R}, \tag{27}$$

where $f_0=1/(\exp(\hbar\omega/k_BT)-1)$ is the equilibrium phonon distribution function, ω is the phonon frequency, and v_x is the x-component of the phonon velocity. To derive the C-V model from the phonon BTE, the integration on moments of the distribution function is needed. By multiplying the $\hbar\omega\tau_R v_x \mathrm{DOS}(\omega)/4\pi$(DOS is the density of phonon state) at both sides of the equation and then integrating them in both the wave vector ($\vec{k}$) space and the frequency (ω) space, the second term in the left side becomes

$$\tau_R\sum_{p=1}^{3}\int_\Omega\int_\omega \hbar\omega v_x^2\frac{\partial f}{\partial x}\frac{DOS(\omega)}{4\pi}d\omega d\Omega, \tag{28}$$

where Ω is the solid angle in wave vector space. Making diffusive approximation on distribution function $f-f_0\ll f_0$ or $f\approx f_0$,[11] Eq. (28) is simplified to

$$\begin{aligned}&\tau_R\sum_{p=1}^{3}\int_\Omega\int_\omega \hbar\omega v_x^2\frac{\partial f}{\partial x}\frac{DOS(\omega)}{4\pi}d\omega d\Omega\\&=\tau_R\sum_{p=1}^{3}\int_\Omega\int_\omega \hbar\omega v_x^2\frac{\partial f_0}{\partial x}\frac{DOS(\omega)}{4\pi}d\omega d\Omega\\&=\lambda\frac{\partial T}{\partial x},\end{aligned} \tag{29}$$

with $\lambda=c_V\rho v^2\tau_R/3=c_V\rho v l/3$. The assumption $v_x^2=v^2/3$, used in getting Eq. (29), is the result of the diffusive approximation, which implies that the distribution function is nearly isotropic in wave vector space. However, for ultrafast process where the system is in highly non-equilibrium state, the distribution function is highly anisotropic.

To modify the diffusive approximation stated above, the high order angular dependence of phonon distribution should be considered. Separate the distribution function to be[47]

$$f(\theta,X)=\rho(\theta)g(X), \tag{30}$$

where $\rho(\theta)$ is the part related to the angle, and $g(X)$ is the part to other variables. It is required for $g(X)$ to satisfy

$$\begin{aligned}&\sum_{p=1}^{3}\int_\Omega\int_\omega \hbar\omega f(\theta,X)\frac{DOS(\omega)}{4\pi}d\omega d\Omega\\&=\sum_{p=1}^{3}\int_\omega \hbar\omega g(X)DOS(\omega)d\omega,\end{aligned} \tag{31}$$

which is actually the requirement for energy conservation: making adiabatic treatment for the phonons with distribution function $f(\theta,X)$ and relaxing them to complete equilibrium state, the distribution function of the final equilibrium state is $g(X)$. By combining Eqs. (30) and (31), the simplified requirement is obtained

$$\begin{cases}f(\theta,X)=\rho(\theta)g(X)\\\dfrac{1}{4\pi}\displaystyle\int_\Omega\rho(\theta)d\Omega=1.\end{cases} \tag{32}$$

Now Eq. (28) can be simplified to be

$$\begin{aligned}&\frac{\partial}{\partial x}\sum_{p=1}^{3}\int_\Omega\int_\omega \hbar\omega f v_x^2\tau_R\frac{DOS(\omega)}{4\pi}d\omega d\Omega\\&={v_q}^2\tau_R\frac{\partial}{\partial x}\sum_{p=1}^{3}\int_\omega \hbar\omega g DOS(\omega)d\omega\frac{1}{4\pi}\int_\Omega\rho(\theta)\cos^2\theta d\Omega\\&=\chi{v_q}^2C_v\tau_R\frac{\partial T}{\partial x}+v_q^2\tau_R C_vT\frac{\partial\chi}{\partial x},\end{aligned} \tag{33}$$

where $\chi=\chi(x,t)=(1/4\pi)\int_\Omega\rho(\theta)\cos^2\theta d\Omega$. Under diffusive approximation, $\chi_0=1/3$. The modified C-V model is then derived

$$\tau_R\frac{\partial q}{\partial t}+\lambda^*\frac{\partial T}{\partial x}+\frac{\partial\lambda^*}{\partial x}T=-q, \tag{34}$$

where $\lambda^*=\chi\tau_R{v_q}^2c_v\rho$ is defined as the effective thermal conductivity which is time- and position-dependent. The wave equation of temperature is obtained by combining Eq. (34) and the energy conservation equation

$$\frac{\partial^2T}{\partial t^2}+\frac{1}{\tau_R}\frac{\partial T}{\partial t}=\frac{1}{\tau_R\rho c_V}\left(\lambda^*\frac{\partial^2T}{\partial x^2}+2\frac{\partial\lambda^*}{\partial x}\frac{\partial T}{\partial x}+T\frac{\partial^2\lambda^*}{\partial x^2}\right). \tag{35}$$

Compared with the wave equation from the C-V model, Eq. (35) includes the terms of derivation of ETC with respect to the position. While the MC simulation in this work is a uniform simulation at micro level, the time- and position-dependent ETC is non-uniform, which is the result of the use

of macroscopic quantity when describing a highly non-equilibrium state or ballistic transport. Detailed discussions are followed in Section III C. The terms caused by the ETC-position dependence are different in magnitudes under different boundary phonon emission conditions and reflect the evolution of angular distribution of the distribution function with the propagation and scattering of phonons. The velocity of the thermal wave predicted by Eq. (35) is

$$v_w{}^* = \sqrt{\chi} v_q = v_w{}^*(x,t), \tag{36}$$

which is a function of time and position. A parameter reflecting the degree of the anisotropy of the phonon system can be defined as

$$\eta = \eta(x,t) = \chi/\chi_0 = 3\chi. \tag{37}$$

The time and position dependence of the wave velocity which caused by the evolution of η would result in the dispersion of the thermal wave similar to what has been pointed out in Ref. 39.

Different boundary phonon emissions in the MC simulations correspond to the different changing processes of the thermal wave velocity in the modified C-V model. The thermal wave propagates with a constant velocity equal to v_q under the DE condition. Actually, the simulations with DE for ballistic transport are described by the phonon BTE with no scattering term and a constant wave vector

$$\frac{\partial f}{\partial t} + v_q \cos(\theta_0)\frac{\partial f}{\partial x} = 0, \tag{38}$$

with a wave solution $f = f(x - v_q \cos(\theta_0)t)$. The thermal wave velocity near the boundary at the beginning under the LE condition could be calculated by considering the analytical solution of the phonon BTE for ballistic transport where the scattering term can be canceled

$$\frac{\partial f}{\partial t} + v_x \frac{\partial f}{\partial x} = 0. \tag{39}$$

The analytical solution is[15]

$$f = f_w[t - (s - s_0)/|\vec{v}|, r - (s - s_0)\hat{\Omega}], \tag{40}$$

which indicates a cosine-form distribution when $f_w = f_0$ is set, where t is the time, $s - s_0$ is the distance along the propagation direction $\hat{\Omega}$, and f_w is the boundary distribution function along the direction $\hat{\Omega}$. According to the way noted by Eq. (32), the distribution function near the boundary at the beginning can be rewritten as the separation form

$$f = 4\cos(\theta) g(X), \tag{41}$$

where the factor 4 is due to the normalization on the hemispherical distribution. The velocity of the thermal wave at the boundary is then obtained

$$v_w{}^* = \sqrt{\chi} v_q = \frac{\sqrt{2}}{2} v_q, \tag{42}$$

where $\chi = (1/4\pi)\int_\Omega \rho(\theta)\cos^2\theta d\Omega = (1/4\pi)\int_\Omega 4\cos^3\theta d\Omega = 1/2$. At time much larger than the phonon relaxation time, phonons transport in diffusive regime, and the thermal wave propagates with a steady velocity equal to $\sqrt{3}v_q/3$. The processes that the velocity changes from $\sqrt{2}v_q/2$ or v_q to $\sqrt{3}v_q/3$ are exactly the developments of the thermal transport from ballistic to diffusive regime.

The modified C-V model is derived and can characterize the evolution of the thermal transport regime. However, the determination of the ETC relies on the exact solutions of the phonon BTE. The most important is that the main property of the modified equation does not change, and the evolution of the thermal wave predicted by the modified model would still be different from that by the MC simulations. The failure of the modification in considering the higher order angular dependence of the phonon distribution indicates the limits of the simple macroscopic equation in describing the ultrafast transient thermal transport.

C. Macroscopic quantities in ballistic transport

In phonon system, the phonon mode is determined specifically by variables $(\omega, \vec{k})$ when the polarizations of phonons are not distinguished. The mean frequency ω_0 under the gray approximation could be calculated to be

$$\omega_0 = \frac{\sum_{p=1}^{3}\int_\omega \omega f DOS(\omega) d\omega}{N_p}, \tag{43}$$

where $N_p = \sum_{p=1}^{3}\int_\omega f DOS(\omega) d\omega$. Now, the function of the phonon frequency spectrum is simplified to be $N_p\delta(\omega - \omega_0)$. For heat flux density

$$\begin{aligned}\vec{q} &= \sum_{p=1}^{3}\int_\Omega\int_\omega \hbar\omega f v_x DOS(\omega) d\omega d\Omega \\ &= \overrightarrow{v_{xa}}\sum_{p=1}^{3}\int_\omega \hbar\omega f DOS(\omega) d\omega \\ &= N_p \hbar\omega_0 \overrightarrow{v_{xa}},\end{aligned} \tag{44}$$

where $\overrightarrow{v_{xa}} = v_{xa}\overrightarrow{k_0}/|\overrightarrow{k_0}|$. The formulas above show that the integration on moments of microscopic quantities is equivalent to averaging phonons on both magnitude and direction of wave vectors, and the information of the phonon distribution in wave vector space is lost due to the integration. The function of frequency spectrum and wave vector is then simplified to be $N_p\delta(\omega - \omega_0)\delta(\vec{k} - \overrightarrow{k_0})$. Thus, the mode is determined as $(\omega_0, \overrightarrow{k_0})$ for a given phonon, and then the thermal motion is decoupled to be monochromatic mechanical waves under a definite frequency and wave vector.

In ballistic transport, the monochromatic waves with single wave vector propagate without resistive scatterings, and the momentum is well kept. In diffusive conditions, the monochromatic waves are submerged in the resistive scatterings as the infinite small control volume in physics is large enough to contain large amount of phonons and the characteristic time is long enough to make sure enough R scattering. Considering the motion of a single phonon emitted from the boundary, the mean square displacements (MSD) in x direction of the phonon experiencing no scattering and

enough scattering (corresponding to the ballistic transport and the diffusive transport) are

$$\overline{x^2} = \overline{(vt\cos\theta)^2} = \frac{1}{2}v^2t^2 \sim t^2, \tag{45}$$

$$\overline{x^2} = \overline{\left(\sum_i^n l\cos\theta_i\right)^2} = \frac{1}{3}nl^2 = \frac{1}{3}lvt \sim t, \tag{46}$$

respectively. Different transport processes correspond to the different $\overline{x^2} - t$ relations, i.e., $\overline{x^2} \sim t^2$ for phonon ballistic transport, $\overline{x^2} \sim t$ for phonon diffusive transport, and $\overline{x^2} \sim t^\alpha (1 < \alpha < 2)$ for ballistic-diffusive transport, which agree with the analyses in Ref. 22 based on the MD simulation results. The difference between the ballistic condition and the diffusive condition is whether the time-averaging of the motion of single phonon is equivalent to its system-averaging except the $\overline{x^2} - t$ relations. As the square displacement of a specific phonon is

$$x^2 = (vt\cos\theta)^2, \tag{47}$$

which depends on both time and direction of the motion, the time-averaging of the motion of single phonon is not equivalent to its system-averaging for ballistic condition. Thus, more information, i.e., the phonon directional information is needed to describe the transport process completely.

Here, the equivalence between the C-V model and the phonon BTE is illustrated. There are eigenvalue method, perturbation method, moment method, and so on to solve the BTE analytically.[48] The moment method requires a function assemble describing the system completely to make sure the equivalence between the moment equations and the BTE. More equations of fluxes and more boundary conditions correspondingly containing derivatives on time and position are needed to ensure the accuracy of the moment method as the Knudsen number becomes larger. The C-V model is derived from BTE by considering the second moments of the distribution function, which can be seen as an application of moment method. While the MC simulation solves the BTE accurately by simulating its corresponding physical processes, the differences between the results of temperature calculated by MC simulations and the C-V model indicate that the C-V model including the modified C-V model is not a good substitute for the phonon BTE in describing the ultrafast thermal transport.

D. Initial and boundary conditions

In this section, the discussion is launched on the boundary conditions of the distribution function to the phonon BTE and the corresponding emissions in MC simulations. As the gray approximation is adopted, the discussion is focused on the phonon angular distribution at the boundary. Once the boundary condition is determined, the emission in MC simulations is determined accordingly by the following relation:[24]

$$G(\theta) = \int_0^\theta \rho(\theta')\cos\theta'\sin\theta' d\theta', \tag{48}$$

where $\rho(\theta')$ is the part of the boundary distribution function relative to the angle only, and $G(\theta)$ is the random quantity distributed from 0 to 1 uniformly which is, namely, the emission function in MC simulations.

For real heating processes, the boundary conditions depend on the types of heating (whether there are interfaces) and also the period, the magnitudes, and the phonon frequency spectrum of the heat pulse.[49] There are two types of pulse heating, one is pulse heating with transducer,[50] and the other is pulse laser heating.[1–4] The effects of the interface need to be considered in heating process with transducer, including the elastic and inelastic scatterings of phonons in transmitting the interface. For inelastic scattering process, the complete phonon frequency spectrums and the dispersion relations are required to be considered.[51] Experimental and theoretical investigations on the angular distribution of phonons from metal film and cleaved {100} face of NaF to liquid helium are taken by Wyatt,[47,49,52–56] and several different angular distributions were measured under different heating conditions. The distribution functions at the boundary can be then fitted with the experimental data of the angular distributions using Eq. (32).[47] For ultra-short pulse laser heating process, phonons are excited by the hot electrons heated by the pulse laser within the skin depth. By assuming that the heat flux has been formed within the skin depth, the boundary condition could be selected to be in the form of $f = f_0 - \tau_R v_x \partial f_0/\partial x$ in which the derivation is determined according to the magnitudes of the heat flux density and the thickness of the skin depth.

IV. CONCLUSIONS

(1) The heat pulse propagates with a finite speed as ballistic thermal wave in both the MC simulations and the C-V model. However, the velocity of the wave front in the predictions of MC simulation is v_q, while $\sqrt{3}v_q/3$ in those of the C-V model. Besides, the temperature profiles are determined under heat flux boundary conditions in the C-V model, while they also depend on the phonon emission directions in the MC simulations. The shapes of the heat pulse barely influence the temperature distributions and cannot be kept during the process of propagation in the MC simulations with LE, while they are well kept in the predictions of the C-V model. The peak value of the temperature profiles of simulations with LE is much lower than that of the C-V model and attenuates rapidly within the first 10 ps (comparable to the phonon relaxation time 11.2 ps).
(2) The temperature profiles calculated by the MC simulations with LE are the cosine-weighted superposition of all possible profiles (emission angle ranges from 0° to 90°) calculated by the simulations with DE. The temperature distributions calculated by the C-V model can be obtained in the MC simulations only with DE by setting phonon velocity $v = \sqrt{3}v_q/3$.
(3) A modified C-V model is derived from the phonon BTE with a time- and position-dependent ETC. The corresponding time- and position-dependent thermal wave

velocity characterizes the evolution of the thermal transport from ballistic to diffusive regime.

(4) The reason why the macroscopic thermal wave model (including the modified C-V model) could not describe the ballistic thermal wave accurately is the failure of the macroscopic quantities when describing the highly non-equilibrium state. The information of the phonon distribution in wave vector space is lost due to the integration on moments of the distribution function in wave vector space, which causes the incompletion of the macroscopic quantities when describing the highly non-equilibrium phonons and their boundary conditions.

(5) The phonon emissions in the MC simulations are determined correspondingly by the boundary conditions of the distribution function for the phonon BTE which are different under different heating conditions. Heating types (whether there are interfaces) and the angular frequency, the magnitude, and the phonon frequency spectrum of the heat pulse all influence the boundary conditions. The temperature distribution and the significant degree of wave characteristics of the heat propagation in ballistic-diffusive regime both depend on the boundary conditions of the distribution function.

ACKNOWLEDGMENTS

This work was financially supported by the National Natural Science Foundation of China (Nos. 51322603, 51136001, and 51356001), the Science Fund for Creative Research Group (No. 51321002), and the Tsinghua National Laboratory for Information Science and Technology of China (TNList).

[1]G. Cahill, W. K. Ford, K. E. Goodson, G. D. Mahan, A. Majumdar, H. J. Maris, R. Merlin, and S. R. Phillpot, J. Appl. Phys. **93**, 793 (2003).
[2]D. G. Cahill, P. V. Braun, G. Chen, D. R. Clarke, S. H. Fan, K. E. Goodson, P. Keblinski, W. P. King, G. D. Mahan, A. Majumdar, H. J. Maris, S. R. Phillpot, E. Pop, and S. Li, Appl. Phys. Rev. **1**, 011305 (2014).
[3]R. R. Gattass and E. Mazur, Nat. Photonics **2**, 219 (2008).
[4]J. Cheng, C. S. Liu, S. Shang, D. Liu, W. Perrie, G. Dearden, and K. Watkins, Opt. Laser Technol. **46**, 88 (2013).
[5]R. M. Costescu, M. A. Wall, and D. G. Cahill, Phys. Rev. B **67**, 054302 (2003).
[6]Y. K. Koh, S. L. Singer, W. Kim, J. M. O. Zide, H. Liu, D. G. Cahill, A. Majumdar, and A. C. Gossard, J. Appl. Phys. **105**, 054303 (2009).
[7]Y. K. Koh, Y. Cao, D. G. Cahill, and D. Jena, Adv. Funct. Mater. **19**, 610 (2009).
[8]J. P. Feser and D. G. Cahill, Rev. Sci. Instrum. **83**, 104901 (2012).
[9]D. D. Joseph and L. Preziosi, Rev. Mod. Phys. **61**, 41 (1989).
[10]D. Y. Tzou, *Macro- to Micro-scale Heat Transfer: The Lagging Behavior* (Taylor and Francis, Washington, DC, 1997).
[11]G. Chen, *Nanoscale Energy Transport and Conversion: A Parallel Treatment of Electrons, Molecules, Phonons, and Photons* (Oxford University Press, 2005).
[12]C. Cattaneo, Atti Semin. Mat. Fis. Univ. Modena **3**, 83 (1948).
[13]M. P. Vernotte and C. R. Hebd, Acad. Sci. Paris **246**, 3154 (1958).
[14]A. Majumdar, J. Heat Transfer **115**, 7 (1993).
[15]G. Chen, Phys. Rev. Lett. **86**, 2297 (2001).
[16]B. Y. Cao and Z. Y. Guo, J. Appl. Phys. **102**, 053503 (2007).
[17]Y. Dong, B. Y. Cao, and Z. Y. Guo, J. Appl. Phys. **110**, 063504 (2011).
[18]M. K. Zhang, B. Y. Cao, and Y. C. Guo, Int. J. Therm. Sci. **84**, 9 (2014).
[19]J. Ordonez-Miranda, R. G. Yang, and J. J. Alvarado-Gil, J. Appl. Phys. **109**, 084319 (2011).
[20]D. H. Tsai and R. A. MacDonald, Phys. Rev. B **14**, 4714 (1976).
[21]T. Kim, M. A. Osman, C. D. Richards, D. F. Bahr, and R. F. Richard, Phys. Rev. B **76**, 155424 (2007).
[22]W. J. Yao and B. Y. Cao, Chin. Sci. Bull. **59**, 3495 (2014).
[23]J. Xu and X. W. Wang, Physica B **351**, 213 (2004).
[24]Y. C. Hua, Y. Dong, and B. Y. Cao, Acta Phys. Sin. **62**, 244401 (2013).
[25]V. Peshkov, J. Phys. (Moscow) **8**, 381 (1944).
[26]C. C. Acherman, B. Bertman, H. A. Fairbank, and R. A. Guyer, Phys. Rev. Lett. **16**, 789 (1966).
[27]C. T. Lane, H. A. Fairbank, and W. M. Fairbank, Phys. Rev. **71**, 600 (1947).
[28]E. W. Prohofsky and J. A. Krumhansl, Phys. Rev. **133**, A1403 (1964).
[29]V. Narayanamurti and R. C. Dynes, Phys. Rev. Lett. **28**, 1461 (1972).
[30]L. D. Landau, J. Phys. (Moscow) **5**, 71 (1941).
[31]R. A. Guyer and J. A. Krumhansl, Phys. Rev. **148**, 778 (1966).
[32]H. F. Hoevers, M. L. Ridder, A. Germeau, M. P. Bruijn, P. A. J. de Korte, and R. J. Wiegerink, Appl. Phys. Lett. **86**, 251903 (2005).
[33]D. Xu, I. Skachko, A. Barker, and E. Y. Andrei, Nat. Nanotechnol. **3**, 491 (2008).
[34]M. Heiblum, M. I. Nathan, D. C. Thomas, and C. M. Knoedler, Phys. Rev. Lett. **55**, 2200 (1985).
[35]F. X. Alvarez and D. Jou, J. Heat Transfer **132**, 012404 (2010).
[36]R. B. Wilson and D. G. Cahill, Nat. Commun. **5**, 5075 (2014).
[37]J. M. Peraud and N. G. Hadjiconstantinou, Appl. Phys. Lett. **101**, 153114 (2012).
[38]Y. C. Hua and B. Y. Cao, Int. J. Heat Mass Transfer **78**, 755 (2014).
[39]M. K. Zhang, B. Y. Cao, and Y. C. Guo, Int. J. Heat Mass Transfer **67**, 1072 (2013).
[40]H. Q. Yang, Numer. Heat Transfer B **18**, 221 (1990).
[41]S. Lee, D. Broido, K. Esfarjani, and G. Chen, Nat. Commun. **6**, 6290 (2015).
[42]H. D. Wang, W. G. Ma, X. Zhang, and Z. Y. Guo, Int. J. Heat Mass Transfer **54**, 967 (2011).
[43]T. Q. Qiu and C. L. Tien, J. Heat Transfer **115**(4), 835 (1993).
[44]S. L. Anisimov, B. L. Kapeliovich, and T. L. Perelman, Sov. Phys. JETP **39**, 375 (1974).
[45]J. G. Fujimoto, J. M. Liu, E. P. Ippen, and N. Bloembergen, Phys. Rev. Lett. **53**, 1837 (1984).
[46]H. D. Wang, W. G. Ma, X. Zhang, and W. Wang, Acta Phys. Sin. **59**, 3856 (2010).
[47]I. N. Adamenko, K. E. Nemchenko, V. A. Slipko, and A. F. G. Wyatt, J. Low Temp. Phys. **157**, 509 (2009).
[48]C. Cercignani, *The Boltzmann Equation and Its Applications* (Springer-Verlag, New York, Inc., 1961).
[49]R. A. Sherlock, A. F. G. Wyatt, N. G. Mills, and N. Lockerbie, Phys. Rev. Lett. **29**, 1299 (1972).
[50]P. C. Kwok, Phys. Rev. **175**, 1208 (1968).
[51]H.-K. Lyeo and D. G. Cahill, Phys. Rev. B **73**, 144301 (2006).
[52]N. G. Mills, A. F. G. Wyatt, and R. A. Sherlock, J. Phys. C: Solid State Phys. **8**, 289 (1975).
[53]R. A. Sherlock, N. G. Mills, and A. F. G. Wyatt, J. Phys. C: Solid State Phys. **8**, 300 (1975).
[54]M. A. H. Tucker and A. F. G. Wyatt, J. Phys.: Condens. Matter **6**, 2813 (1994).
[55]M. A. H. Tucker and A. F. G. Wyatt, J. Phys.: Condens. Matter **6**, 2825 (1994).
[56]D. H. S. Smith and A. F. G. Wyatt, Phys. Rev. B **76**, 224519 (2007).